

Analytical classical density functionals from an equation learning network

S.-C. Lin,^{1, a)} G. Martius,² and M. Oettel¹

¹⁾*Institut für Angewandte Physik, Eberhard Karls Universität Tübingen, 72076 Tübingen, Germany*

²⁾*Max Planck Institute for Intelligent Systems Tübingen, 72076 Tübingen, Germany*

We explore the feasibility of using machine learning methods to obtain an analytic form of the classical free energy functional for two model fluids, hard rods and Lennard–Jones, in one dimension. The Equation Learning Network proposed in Ref. 1 is suitably modified to construct free energy densities which are functions of a set of weighted densities and which are built from a small number of basis functions with flexible combination rules. This setup considerably enlarges the functional space used in the machine learning optimization as compared to previous work² where the functional is limited to a simple polynomial form. As a result, we find a good approximation for the exact hard rod functional and its direct correlation function. For the Lennard–Jones fluid, we let the network learn (i) the full excess free energy functional and (ii) the excess free energy functional related to interparticle attractions. Both functionals show a good agreement with simulated density profiles for thermodynamic parameters inside and outside the training region.

I. INTRODUCTION

Density functional theory (DFT) may be viewed as a great reductionist scheme for classical and quantum many–body systems in equilibrium. The one–to–one correspondence between the one–body density profile of particles and the one–body external potential acting on these particles entails that a unique (free) energy functional of the one–body density contains all of the homogeneous and inhomogeneous equilibrium structure in a given system, and no explicit knowledge of higher–order correlations (i.e. through the phase space distribution of classical particles or the full many–body quantum wavefunction) is needed.

In general, the analytical form of the (free) energy functional is unknown, except for a handful of particular model systems (mostly in one dimension [1D]). In recent years, some effort has gone into approximating (“learning”) functionals by machine learning (ML) techniques. In quantum DFT, e.g., interpolating functionals generated by kernel ridge regression have been tested for model 1D systems^{3,4} and also have been extended to 3D systems⁵. Numerically interpolated functionals do not contain sufficient information about functional gradients, therefore both the energy–density map and the external potential–density maps had to be learned by interpolation⁴. For the 1D Hubbard model, a convolutional network functional has been learned whose numerical functional derivative appears to be more robust⁶. However, these approaches hide the energy functional inside an “ML black box” which does not permit much insight from a theory perspective. For the classical case, a 1D LJ like fluid was studied with a convolutional network², utilizing an established approach from liquid state theory of splitting the excess free energy functional into a “repulsion” part and an “attraction” part \mathcal{F}^{att} . The convolutional network naturally led to an approximation of \mathcal{F}^{att} in terms of weighted densities n_i , which are the essential building blocks in modern classical DFT; however, the free energy density $f^{\text{att}}(n_i)$ as a function of n_i had to be prescribed as simple polynomials. An interpretable results obtained in² was the

accurate splitting of the interaction potential in the Weeks–Chandler–Andersen (WCA) spirit⁷.

In this context, the question naturally arises whether ML techniques can be used to learn analytic forms of (free) energy functionals instead of “black boxes” or presumed forms. This question is important also in a more general context: can ML algorithms contribute to theory building in physics? In the ML community, efforts in that direction have utilized genetic algorithms to search a space of simple basis function with multiplication and addition rules⁸. More recent work proposes an equation learning network employing gradient-based optimization with simple basis functions and division besides multiplication/addition as combination rules^{1,9}. An empirical principle for the “right” formula (choose the simplest one that still predicts well, i.e. Occam’s razor) can be built into the cost function. This principle was also successful in the history of physics in finding analytical models with high predictive power even outside the training/observed regime. For the DFT problem, the extrapolation power to other external potentials is an important aspect, as well as the analytic differentiability of the free energy functional since structural information about the fluid (pair correlations) is obtained via the direct correlation function (two functional derivatives of the excess free energy functional). These aspects are explored below for the model cases of a hard rod (HR) and a Lennard–Jones (LJ) fluid in 1D.

II. CLASSICAL DFT

In classical DFT, the grand potential functional of 1D system is

$$\Omega[\rho(x)] = \mathcal{F}^{\text{id}}[\rho(x)] + \mathcal{F}^{\text{ex}}[\rho(x)] + \int dx (V^{\text{ext}}(x) - \mu)\rho(x), \quad (1)$$

where $\rho(x)$ is the particle density distribution, \mathcal{F}^{id} is the free energy functional of the ideal gas, \mathcal{F}^{ex} is the excess free energy functional (unique for a given pair potential between particles), μ is the chemical potential and V^{ext} is an external po-

^{a)}Electronic mail: shang-chun.lin@uni-tuebingen.de

tential. The exact form of \mathcal{F}^{id} is:

$$\beta \mathcal{F}^{\text{id}} = \int dx \rho(x) [\ln(\rho(x)\lambda) - 1] \quad (2)$$

with $\beta = 1/(k_B T)$, T the temperature, k_B Boltzmann's constant, and λ the thermal wavelength. In the following we set $\beta = \lambda = 1$.

In equilibrium, the corresponding density profile ρ^{eq} minimizes Ω for a given μ . Thus, with $\frac{\delta \Omega}{\delta \rho} = 0$ and Eq. (2), we obtain

$$\rho^{\text{eq}} = \exp\left(\mu - \frac{\delta \mathcal{F}^{\text{ex}}}{\delta \rho} \Big|_{\rho=\rho^{\text{eq}}} - V^{\text{ext}}\right). \quad (3)$$

All DFT solutions for test density distributions in this work are obtained by iteratively solving Eq. (3) using the Picard method with mixing.

In this paper, we investigate the HR pair potential:

$$U_{\text{HR}}(x) = \begin{cases} \infty & \text{if } x < \sigma \\ 0 & \text{otherwise} \end{cases}$$

as well as the LJ(-like) potential:

$$U_{\text{LJ}}(x) = \begin{cases} \infty & \text{if } x < \sigma \\ 4\epsilon \left[\left(\frac{\sigma}{x}\right)^{12} - \left(\frac{\sigma}{x}\right)^6 \right] & \text{if } \sigma < x < 16\sigma \\ 0 & \text{otherwise} \end{cases}$$

with x the distance between particle centers, σ the diameter of the particles and ϵ the strength of interaction. In the following we set $\sigma = 1$.

III. MACHINE LEARNING

A. Model

We define a machine learned excess free energy functional \mathcal{F}^{ML} and the resulting ML output density ρ^{ML} by

$$\rho^{\text{ML}}(x) = \exp\left(\mu^{\text{ML}} - \frac{\delta \mathcal{F}^{\text{ML}}}{\delta \rho} \Big|_{\rho=\rho^{\text{ML}}} - V^{\text{ext}}\right). \quad (4)$$

This is the equivalent of a ‘‘generative step’’ of a learned distribution ρ^{ML} from an input distribution ρ^{eq} in an ML network (via weighted densities n_i , see below). Here, μ^{ML} is chosen to minimize the difference between ρ^{eq} and ρ^{ML} (see Ref. 2 for details).

The network we propose, Functional Equation Learner (FEQL), is a L -layered feed-forward network with computational units specifically designed for constructing the free energy functional (see Fig. 1). The first layer consists of convolution kernels which compute the weighted densities n_i with the convolution kernel ω_i ($i = 1 \dots n_w$) by

$$n_i(x) = \rho \otimes \omega_i = \int dx' \rho(x') \omega_i(x - x'), \quad (5)$$

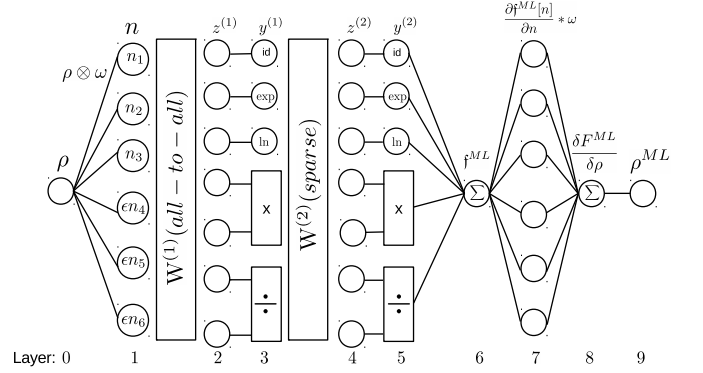


FIG. 1: Network architecture of the proposed FEQL for 10 layers ($L = 9$) and one neuron per type ($u = 3$, $v = 2$) and 6 convolution (weighting) kernels ($n_w = 6$). ϵ is the coupling strength (equivalent to inverse temperature) in the LJ potential.

and some of the weighted densities are multiplied by ϵ in the case of the LJ fluid. Using weighted densities instead of the particle density is inspired by the exact HR functional¹⁰ and fundamental measure theory^{11,12}. The layer 2 is a linear, all-to-all mapping of the vector (of functions) $n = \{n_i(x)\}$ to the vector

$$z^{(l=1)} = W^{(1)} n \quad (6)$$

at level $l = 1$. The layers $3 \dots L - 4$ are a sequence of nonlinear and linear transformations. The non-linear transformation at level l contains u unary units f_i and v binary units g_J and maps $z^{(l)}(x)$ ($u + 2v$ -dimensional) to the layer output $y^{(l)}$ ($u + v$ -dimensional) as:

$$y^{(l)} := \left(f_1(z_1^{(l)}), f_2(z_2^{(l)}) \dots f_u(z_u^{(l)}), \right. \\ \left. \left(g_1(z_{u+1}^{(l)}, z_{u+2}^{(l)}) \dots g_v(z_{u+2v-1}^{(l)}, z_{u+2v}^{(l)}) \right) \right). \quad (7)$$

The unary units, f_1, \dots, f_u receive the respective component, z_1, \dots, z_u as inputs, and each unit is one of the following base functions indexed by $I \in 0, 1, 2$:

$$f_I(z_i) := \begin{cases} z_i & \text{if } I = 0 \\ \exp(z_i) - 1 & \text{if } I = 1 \\ \ln(z_i + 1) & \text{if } I = 2 \end{cases}$$

The binary units, g_1, \dots, g_v receive the remaining component, z_{u+1}, \dots, z_{u+2v} , as input in pairs of two, and each unit may be multiplication or division indexed by $J \in 0, 1$:

$$g_J(z_i, z_{i+1}) := \begin{cases} z_i \times z_{i+1} & \text{if } J = 0 \\ z_i \div (z_{i+1} + 1) & \text{if } J = 1 \end{cases}$$

Note that $f_I(0) = g_J(0, z) = 0$.

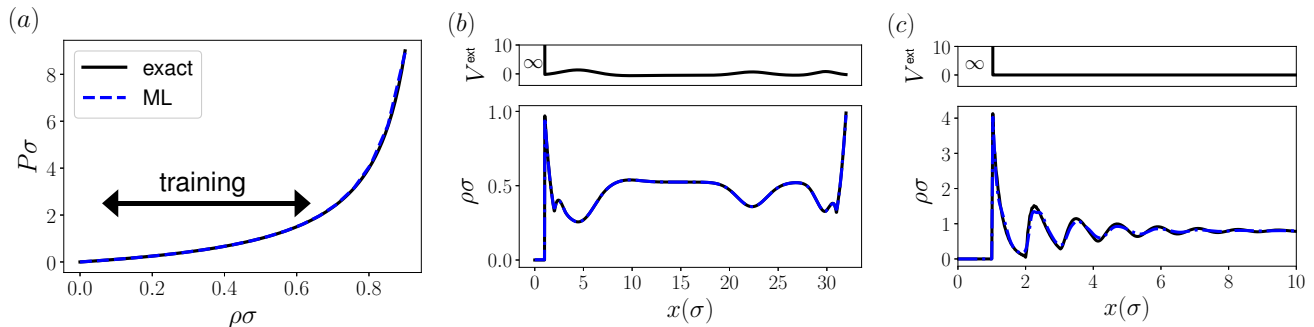


FIG. 2: FEQL results for hard rods. Dark solid lines are exact solutions from \mathcal{F}^{HR} and blue dashed lines are ML results. (a) eos, $P(\rho)$. (b) density profile for $\rho_0 = 0.49$ inside the training region but V^{ext} not in the training data. (c) density profile at hard wall for $\rho_0 = 0.80$ outside the training region.

The linear transformation from level l to $l+1$ maps the $(u+v)$ -dimensional input $y^{(l)}$ to the $(u+2v)$ -dimensional intermediate representation $z^{(l+1)}$ given by

$$z^{(l+1)} = W^{(l+1)}y^{(l)}. \quad (8)$$

Thus, the n_w convolution kernels $\omega(x)$ in the first layer and the matrices $W^{(l)}$ are free parameters that are learned during training.

The machine-learned free energy density f^{ML} is a summation of the output of layer $L-4$, the functional derivative $\frac{\delta \mathcal{F}^{\text{ML}}}{\delta \rho} = \sum_i \frac{\partial f_i^{\text{ML}}}{\partial n} * \omega_i$ (with $\mathcal{F}^{\text{ML}} = \int dx f^{\text{ML}}(n)$ and $*$ denoting cross-correlation) is used in the final, generative step (Eq. (4)). More details about constructing FEQL can be found in the SI.

B. Network training

To obtain training data for ρ^{eq} , grand canonical simulation are used in the case of LJ fluid; for the HR fluid, Eq. (3) is directly solved, since the exact functional is known.

FEQL is fully differentiable in its free parameters $\theta = [W, \omega]$ and can thus be trained using back-propagation. We adopt the following loss function

$$L = \frac{1}{N} \sum_{i=1}^N \left(\alpha_1 \int |\rho_i^{\text{eq}} - \rho_i^{\text{ML}}| dx + \alpha_2 |\mu_i^{\text{eq}} - \mu_i^{\text{ML}}| \right) + \lambda_1 \sum_i \int dx |\omega_i| + \lambda_2 \sum_{l,\alpha\beta} |W_{\alpha\beta}^{(l)}|, \quad (9)$$

with $\alpha_1 = 0.9$ and $\alpha_2 = 0.1$. For training we choose Adam¹³ with mini-batches:

$$\theta_{t+1} = \theta_t + \text{Adam} \left(\frac{\partial L(D(t))}{\partial \theta}, \alpha \right) \quad (10)$$

with α the stepsize parameter (learning rate) and $D(t)$ the data in the current mini-batch. The choice of Adam is not critical and standard stochastic gradient descent also works.

Following Sahoo *et al.*⁹, we adopt a three-step training procedure. At the beginning, we use no regularization ($\lambda_1 = \lambda_2 =$

0), such that parameters can vary freely and reach reasonable starting points. In step 2, we switch on the regularization by setting λ_1 and λ_2 to positive finite values to sparsify the network for obtaining a simpler functional. In step 3, we clamp small parameters with $|W_{\alpha\beta}^{(l)}| < w_{\text{th}}$ to zero. In this way we keep the sparsity introduced by the lasso¹⁴ training in step 2 but make sure unbiased parameter values are attained. In this paper we choose $\alpha = 10^{-3}$, $\lambda_1 = 10^{-7}$ and $w_{\text{th}} = 0.05$.

IV. RESULT

A. Hard rods

The exact equation of state (eos) for the hard rod (HR) fluid is given by pressure $P(\rho) = \frac{\rho}{1-\rho}$ and the analytic form of \mathcal{F}^{HR} (Percus functional) is one of the few known ones^{10,12}.

The parameter of \mathcal{F}^{ML} are trained using 1024 density profiles in a hard wall slit of width 32σ with 3 additional Gaussian potentials of random strength/width and location inside the slit and with a range of training reservoir densities $\rho_0 = 0.2 \dots 0.55$. We choose $n_w = 3$ and (1,1,1,3,1) nodes for (identity, exponential, logarithm, multiplication and division) with $L = 10$ layers (see Fig. 1) and $\lambda_2 = 8 \cdot 10^{-5}$ in Eq. (9) (results for different λ_2 and arguments for an optimal choice are shown in the SI). \mathcal{F}^{ML} is not of the form of the Percus functional, since the convolution kernels of the latter are Dirac delta and Heaviside step functions, which are hard to be captured by our network.

In Fig.2, we show the eos, a density profile inside the thermodynamic training region but not in the training data ($\rho_0 = 0.49$) and a density profile outside the training region ($\rho_0 = 0.80$). The FEQL recovers the almost exact result inside the training region and also performs quite well even outside the training region. The virial expansion

$$P^{\text{ML}}(\rho) \simeq \rho + 1.04\rho^2 + 0.63\rho^3 + \mathcal{O}(\rho^4) \quad (11)$$

of the ML eos shows moderate deviation compare to the exact one ($\frac{\rho}{1-\rho} = \rho + \rho^2 + \rho^3 \dots$); note that no explicit information about the eos is incorporated into the cost function.

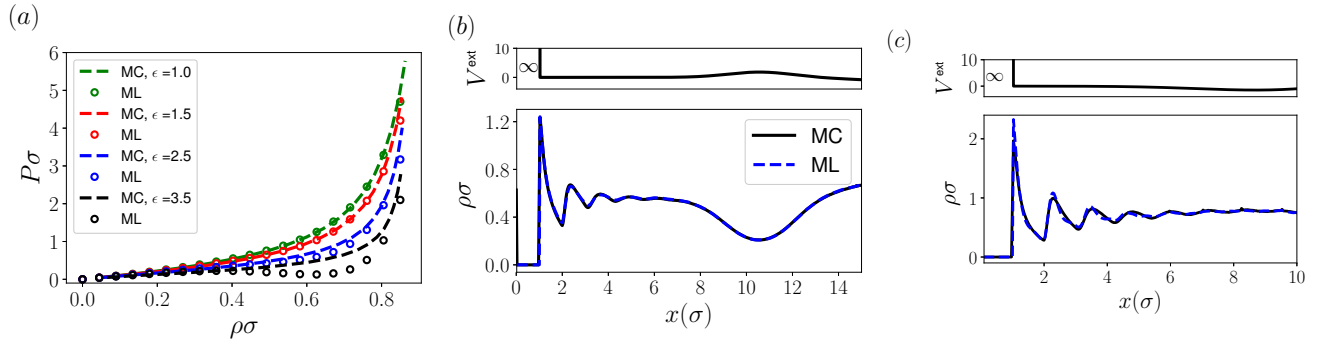


FIG. 3: FEQL results for LJ fluid with functional splitting. (a) eos $P(\rho)$. (b) density profile for $\epsilon=1.30$, $\mu=\ln(1.27)$ inside the training region but V^{ext} not in the training data. (c) density profile for $\epsilon=1.7$, $\mu=\ln(1.7)$, outside the training region. Dark solid lines are simulation profiles and blue dashed lines are ML results.

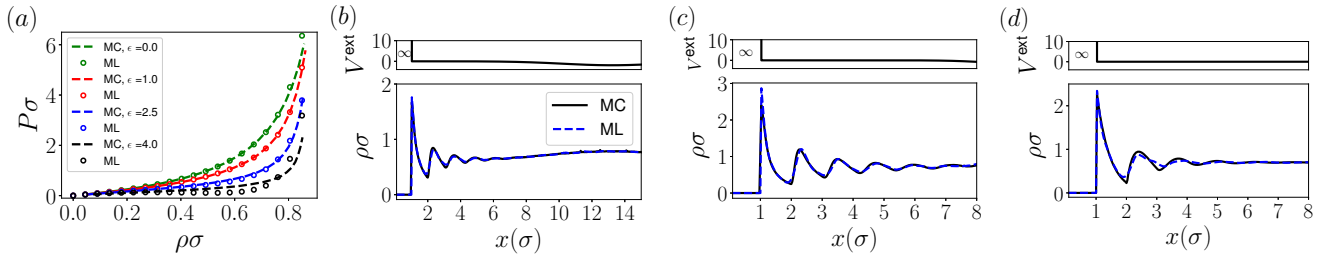


FIG. 4: FEQL results for LJ fluid (no splitting). (a) eos $P(\rho)$. (b) density profile for $\epsilon=1.37$, $\mu=\ln(1.90)$ inside the training region but V^{ext} not in the training data. (c,d) density profile at a hard wall for $\epsilon=1.9$, $\mu=\ln(1.9)$ (c) and $\epsilon=0$, $\rho_0=0.7$ (HR limit, (d)). Dark solid lines are simulation profiles and blue dashed lines are ML results.

B. Lennard–Jones

Here, 1115 training distributions are generated with random μ and ϵ in the range of $0.5\dots 1.5$ and $\ln 0.5\dots \ln 2$, respectively, with V^{ext} prescribed as in the hard rod case. The training data are obtained by grand canonical Monte Carlo (GCMC) simulation.

1. Splitting between repulsions and attractions

Following liquid state theory², we split \mathcal{F}^{ex} into a contribution from repulsions and one from attractions (to be learned by the network) as follows:

$$\mathcal{F}^{\text{ex}} = \mathcal{F}^{\text{HR}} + \epsilon \mathcal{F}^{\text{ML}}, \quad (12)$$

where the factor ϵ makes sure $\mathcal{F}^{\text{ex}}(\epsilon \rightarrow 0) = \mathcal{F}^{\text{HR}}$. Here, in the first layer, we choose $n_w = 4$, 1 kernel multiplied by ϵ and another 3 without this factor (see Fig. 1), and (1,1,1,2,1) nodes for (identity, exponential, logarithm, multiplication and division). The training parameter $\lambda_2 = 5 \cdot 10^{-5}$ in Eq. (9). Results are shown in Fig. 3. The findings are similar to the HR case with a very good match to simulation data for the eos and test distributions inside and outside the thermodynamic training region. For a 1D system with hard-core repulsive and finite range attractive pair potential, the pressure must be monotonically increasing for arbitrary low temperature (high ϵ), and

thus resulting no gas–liquid transition¹⁵. The corresponding ML pressure shows no van der Waals (vdW) loop for attractions strengths up to $\epsilon=3.0$, this is a qualitative step forward as compared to Ref. 2.

2. No splitting

As a further test of the capability of FEQL, we forego the splitting of the functional such that $\mathcal{F}^{\text{ex}} = \mathcal{F}^{\text{ML}}$. In the first layer, we choose $n_w = 6$, 3 kernels multiplied with ϵ and another 3 without this factor, and (1,1,1,3,1) nodes for (identity, exponential, logarithm, multiplication and division). The training parameter $\lambda_2 = 5 \cdot 10^{-5}$ in Eq. (9). For the training data we also include density profiles from the HR case. In Fig. 4, we show the results. Test distributions match well to simulation data both in the HR limit and the regime of higher attractions. The eos shows an unphysical vdW loop for attractions strengths $\epsilon > 3.7$, much higher than the upper limit of the training data.

A modified virial expansion up to second order in ϵ and ρ is given. For the splitting case,

$$P^{\text{ML}}(\rho) = \rho + (-0.01 \epsilon^2 - 1.07 \epsilon + 1) \rho^2 + O(\rho^3) \quad (13)$$

for the no splitting case,

$$P^{\text{ML}}(\rho) = \rho + (-0.06 \epsilon^2 - 0.58 \epsilon + 1.04) \rho^2 + O(\rho^3) \quad (14)$$

and mean-field approximation

$$\mathcal{F}^{\text{ex}} = \mathcal{F}^{\text{HR}} + \frac{1}{2} \int \int_{|x-x'| > \sigma} U_{\text{LJ}}(x-x') \rho(x) \rho(x') dx' dx \quad (15)$$

gives $P^{\text{MF}}(\rho) = P^{\text{HR}}(\rho) - 0.44 \epsilon \rho^2$.

C. Direct correlation function

The direct correlation function (dcf) in DFT is the second functional derivative of \mathcal{F}^{ex} :

$$C^{(2)}(x_1, x_2; \rho_0) = -\frac{\beta \delta^2 \mathcal{F}^{\text{ex}}}{\delta \rho(x_1) \delta \rho(x_2)}, \quad (16)$$

and it depends only on $x = |x_1 - x_2|$ in the case of a homogeneous fluid with density ρ_0 .

As the network is only trained on the level of the first functional derivative (see Eq. 4), it will be a challenge for FEQL to capture the dcf. In Fig. 5, we show exemplary dcf's at moderate to high density for the exact HR functional, LJ from simulation and the corresponding ML results. The direct correlations inside the hard core are captured very well by ML in the HR case and for LJ. However, in the HR case, the $C^{(2)}$ from the ML correctly shows insignificant correlation outside the hard core. In the case of LJ, the contribution to $C^{(2)}$ from attraction is semi-quantitatively correct, with a better result in the splitting case.

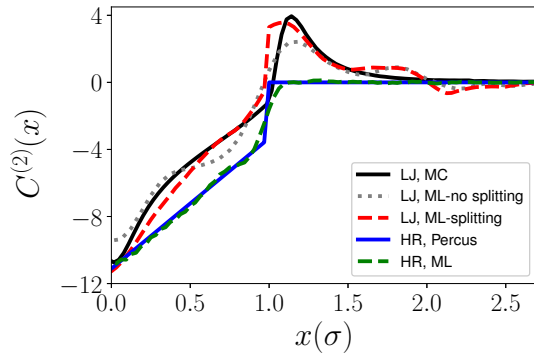


FIG. 5: $C^{(2)}(x, \rho_0)$ with $\rho_0 = 0.7$ (HR) and 0.703 (LJ), $\epsilon = 1.85$ and $\mu = \ln(1.85)$.

V. CONCLUSION

The adaptation of EQL⁹ to the classical DFT problem of finding \mathcal{F}^{ex} has shown satisfactory results for the exemplary case of the 1D HR and LJ fluid. The new network FEQL is very flexible and goes significantly beyond the polynomial

ansatz used in Ref. 2. The analytic form allows for more easily transferable output and further calculations to obtain, e.g., direct correlation functions. An application to more realistic systems in 3D and perhaps also complex fluids such as water appears to be promising^{16–18}. From the results of this work we conclude that the incorporation of results from liquid state theory is not essential here; however, it increases the reliability and trainability of the ML functional. Future work should include information on virial or high density expansions as well as correlation functions (via test particles) and should develop more quantitative measures for extrapolative capabilities of ML functionals.

SUPPLEMENTARY INFORMATION

See supplementary information for the explicit \mathcal{F}^{ML} , convolution kernels $\omega(x)$ and more discussion about FEQL and training procedure.

ACKNOWLEDGMENTS

The authors acknowledge support by the High Performance and Cloud Computing Group at the Zentrum für Datenverarbeitung of the University of Tübingen, the state of Baden-Württemberg through bwHPC and the German Research Foundation (DFG) through grant no INST 37/935-1 FUGG. Further, the work was supported by DFG through the grant OE 285/5-1.

¹G. Martius and C. H. Lampert, arXiv:1610.02995 (2016).

²S.-C. Lin and M. Oettel, SciPost Phys. **6**, 025 (2019).

³J. C. Snyder, M. Rupp, K. Hansen, K.-R. Müller, and K. Burke, Phys. Rev. Lett. **108**, 253002 (2012).

⁴L. Li, J. C. Snyder, I. M. Pelaschier, J. Huang, U.-N. Niranjan, P. Duncan, M. Rupp, K.-R. Müller, and K. Burke, Int. J. Quantum Chem. **116**, 819 (2016).

⁵F. Brockherde, L. Vogt, L. Li, M. E. Tuckerman, K. Burke, and K.-R. Müller, Nat. Commun. **8**, 872 (2017).

⁶J. Nelson, R. Tiwari, and S. Sanvito, Phys. Rev. B **99**, 075132 (2019).

⁷M. Bishop, Am. J. Phys. **52**, 158 (1984).

⁸M. Schmidt and H. Lipson, Science **324**, 81 (2009).

⁹S. S. Sahoo, C. H. Lampert, and G. Martius, in *Proceedings of the 35th International Conference on Machine Learning*, Vol. 80 (PMLR, 2018) pp. 4439–4447.

¹⁰J. K. Percus, J. Stat. Phys. **15**, 505 (1976).

¹¹Y. Rosenfeld, Phys. Rev. Lett. **63**, 980 (1989).

¹²R. Roth, J. Phys. Condens. Matter **22**, 063102 (2010).

¹³D. P. Kingma and J. Ba, arXiv:1412.6980 (2014).

¹⁴R. Tibshirani, J. R. Stat. Soc. Series B Stat. Methodol. , 267 (1996).

¹⁵J. A. Cuesta and A. Sánchez, J. Stat. Phys. **115**, 869 (2004).

¹⁶V. P. Sergiievskiy, G. Jeanmairet, M. Levesque, and D. Borgis, J. Phys. Chem. Lett. **5**, 1935 (2014).

¹⁷G. Jeanmairet, M. Levesque, R. Vuilleumier, and D. Borgis, J. Phys. Chem. Lett. **4**, 619 (2013).

¹⁸G. Jeanmairet, M. Levesque, and D. Borgis, J. Chem. Phys. **139**, 154101 (2013).

Supporting Information:

Analytical classical density functionals from an equation learning network

S.-C. Lin,^{1, a)} G. Martius,² and M. Oettel¹

¹⁾*Institut für Angewandte Physik, Eberhard Karls Universität Tübingen,
72076 Tübingen, Germany*

²⁾*Max Planck Institute for Intelligent Systems Tübingen, 72076 Tübingen,
Germany*

^{a)}Electronic mail: shang-chun.lin@uni-tuebingen.de

I. EXACT HARD ROD FUNCTIONAL

The exact form of the excess free energy functional for hard rods (HR) \mathcal{F}^{HR} is^{1,2}

$$\mathcal{F}^{\text{HR}} = \int \phi[n] dx = \int -n_0 \ln(1 - n_1) dx \quad (1)$$

with $n_i(x) = \rho \otimes \omega_i^{\text{HR}}$ (convolution), where $\omega_1^{\text{HR}}(x) = \theta(\sigma/2 - |x|)$ and $\omega_0^{\text{HR}}(x) = \frac{1}{2}\delta(\sigma/2 - |x|)$. Here, σ is the length of the rod, $\theta(x)$ is the Heaviside step function and $\delta(x)$ the Dirac delta function. Thus,

$$\frac{\delta \mathcal{F}^{\text{HR}}}{\delta \rho} = \sum_i \frac{\partial \mathcal{F}^{\text{HR}}[n]}{\partial n_i} * \omega_i^{\text{HR}}. \quad (2)$$

with $*$ denoting cross-correlation. Eqs. (2) and (1) are used to generate the training profiles in the HR case. In the Lennard–Jones (LJ) case, \mathcal{F}^{HR} describes the repulsive part of the free energy functional.

II. HARD RODS: LEARNING PROCEDURE AND DEPENDENCE ON LOSS FUNCTION PARAMETER λ_2

In the main paper, we have defined the loss function

$$L = \frac{1}{N} \sum_{i=1}^N \left(\alpha_1 \int |\rho_i^{\text{eq}} - \rho_i^{\text{ML}}| dx + \alpha_2 |\mu_i^{\text{eq}} - \mu_i^{\text{ML}}| \right) + \lambda_1 \sum_i \int dx |\omega_i| + \lambda_2 \sum_{l, \alpha\beta} |W_{\alpha\beta}^{(l)}|. \quad (3)$$

The first term quantifies the deviation between generated and input density profile (ground truth) and the corresponding chemical potentials. The second term is a regularizer to avoid numerically large weight functions during the training procedure, and it is not very important for final results. The third term with coefficient λ_2 is used as a substitute for the number of nonzero entries in the matrices $W^{(l)}$ which is not differentiable directly. Nevertheless minimizing the absolute norm tends to produce sparse solutions, see also Lasso regression³, and thus favors simpler functionals.

Before training, we prepare 1024 density profile and randomly divided into 921 density profiles as training set and 103 as validating set. The training procedure only uses training set for updating trainable parameters and evaluates the value of the loss on the training set and on the validating set (called training loss and validation loss) at the end of each iteration⁴. Then, as described in the main paper, we have used a three-step training procedure. In Fig. 1 we show the evolution of the training and validation loss throughout the training for 4

different values of λ_2 . For the higher values of λ_2 (10^{-2} and 10^{-3}) there is a marked increase of L at the beginning of step 2. For $\lambda = 10^{-4}$ the beginning of step 2 without increase of L and then further decreases.

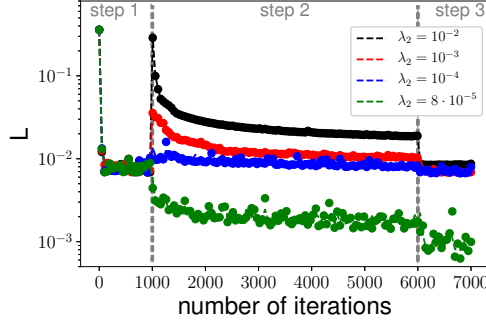


FIG. 1: Loss as a function of number of iterations for 4 different values of λ_2 . Dashed lines are validation loss and solid circles are training loss.

This is further confirmed in the Fig. 2a, which shows the final value of L from the training and validating set as a function of λ_2 . Near-optimal choices are $\lambda_2 < 10^{-4}$. The complexities (the number of nonzero entries in W) increase with decreasing of λ_2 (Fig. 2b). For a broad range of complexities, the validation loss is almost constant (Fig. 2c).

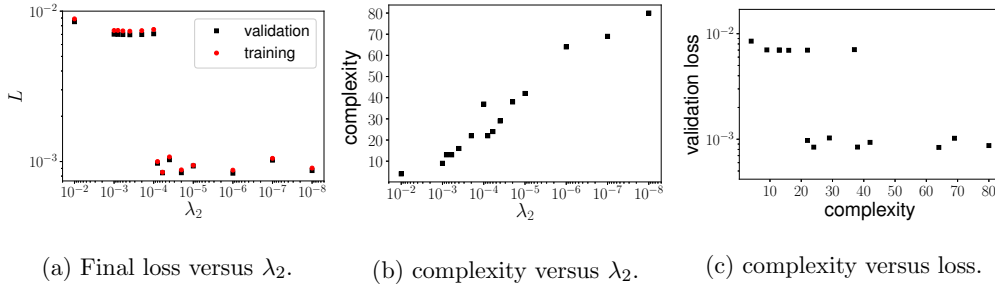
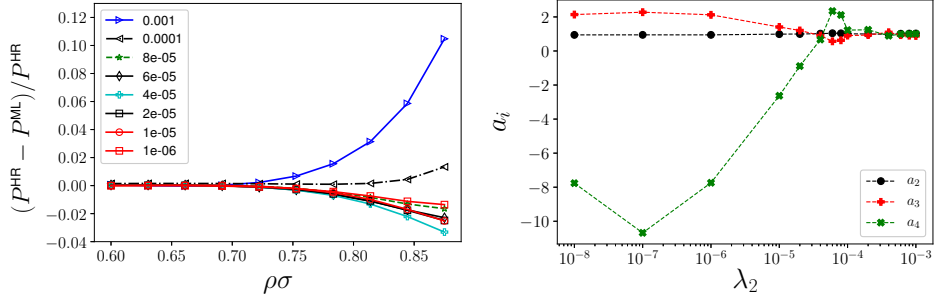


FIG. 2: The interdependence of loss, complexity and λ_2 .

The effect of λ_2 on the bulk equation of state (eos) is shown in Fig. 3. The relative deviation of the ML pressure from the exact one (Fig. 3a) is close to zero for $\lambda_2 < 10^{-3}$. In Fig. 3b we analyze the virial coefficients $a_2 \dots a_4$ ($P = \sum_{i=1} a_i \rho^i$, $a_1 = 1$ (ideal gas) and all $a_i = 1$ for the exact eos). Therefore, we finally choose $\lambda_2 = 8 \cdot 10^{-5}$ as a near-optimal compromise between low loss, complexity and eos.



(a) The relative pressure difference as a function of density ρ . (b) Second to fourth virial coefficient as a function of λ_2 .

FIG. 3: Properties of the bulk fluid: pressure and virial coefficients.

III. FULL \mathcal{F}^{ML}

Here we show the full functional of $\mathcal{F}^{\text{ML}}[n]$, with $n_i(x) = \int dx' \rho(x') \omega_i(x - x')$. The coefficients in \mathcal{F}^{ML} are single precision; for displaying purposes, all coefficients are rounded to the first non-zero digit and then rationalized. For \mathcal{F}^{ML} with full digits, we provide `test_function.ipynb` (*Jupyter notebook*). Also, in `test_function.ipynb` and other notebooks, we demonstrate how to use trained functional to obtain equilibrium density profiles, eos, and direct correlation function.

A. \mathcal{F}^{ML} for hard rod

The FEQL result for hard rod is

$$\mathcal{F}^{\text{ML}} = \int dx \frac{2n_1 y_0 \left(-\frac{7n_0 y_1}{10} + \frac{n_1 y_0}{5} - \frac{9y_2}{10y_3} \right)}{5} - \frac{n_1 y_0}{10} + \frac{\frac{n_0 y_1}{2} - \frac{3n_1 y_0}{10}}{\frac{3n_1 y_0}{5} + 1 + \frac{2y_2}{5y_3}} + \ln \left(-\frac{n_1 y_0}{10} + 1 \right) - 1 + e^{-\frac{n_1 y_0}{5}} \quad (4)$$

with $y_0 = -\frac{n_0}{10} - \frac{3n_1}{5}$, $y_1 = -\frac{n_0}{5} - \frac{9n_2}{10}$, $y_2 = \frac{7n_0}{10} - \frac{2n_1}{5}$, $y_3 = 1 - \frac{2n_1}{5}$ and convolution kernels ω_i shown in Fig.4a.

B. \mathcal{F}^{ML} for LJ with splitting

$\mathcal{F}^{\text{ex}} = \mathcal{F}^{\text{HR}} + \epsilon \mathcal{F}^{\text{ML}}$, where

$$\begin{aligned} \mathcal{F}^{\text{ML}} = & \int dx \left(-\frac{n_2}{10} + \frac{y_0 y_1}{10} + \frac{2 \ln y_2}{5} - \frac{3y_3}{10y_4} \right) \left(\frac{n_2}{10} - \frac{y_0 y_1}{10} - \frac{2 \ln y_2}{5} + \frac{3y_3}{10y_4} \right) \\ & + \left(\frac{n_2}{10} - \frac{y_0 y_1}{10} - \frac{2 \ln y_2}{5} + \frac{3y_3}{10y_4} \right) \left(-\frac{n_1}{10} - \frac{n_2}{10} + \frac{y_0 y_1}{10} + \frac{2 \ln y_2}{5} - \frac{3y_3}{10y_4} \right) \\ & + e^{\frac{2y_0 y_1}{5}} + \ln \left(\frac{y_0 y_1}{2} + 1 \right) - 1 \end{aligned} \quad (5)$$

with

$$\begin{aligned} y_0 &= \frac{\epsilon n_3}{5} + \frac{3n_0}{5} - \frac{3n_1}{5}, \quad y_1 = \frac{7\epsilon n_3}{10} + \frac{n_0}{2} - \frac{n_1}{2}, \quad y_2 = \frac{4\epsilon n_3}{5} + \frac{3n_0}{10} - \frac{3n_1}{5} - \frac{n_2}{2} + 1, \\ y_3 &= \frac{7\epsilon n_3}{5} + \frac{n_1}{5} + \frac{3n_2}{10}, \quad y_4 = -\frac{2n_0}{5} - \frac{n_1}{10} + 1 \end{aligned}$$

and convolution kernels ω_i shown in Fig.4b

C. \mathcal{F}^{ML} for LJ without splitting

The result of \mathcal{F}^{ex} given by FEQL is

$$\begin{aligned} \mathcal{F}^{\text{ML}} = & \int dx \frac{y_0 \ln y_1}{10} + \frac{y_2 y_3}{10} + \frac{-\frac{y_4 y_5}{2} + \frac{3y_2 y_3}{10} - \frac{y_6 y_7}{2}}{\frac{3y_4 y_5}{10} + \frac{3 \ln y_1}{10} + 1} + \left(-\frac{y_4 y_5}{5} + \frac{17e^{y_8}}{10} + \frac{4 \ln y_1}{5} - \frac{17}{10} \right) \\ & \left(-\frac{3\epsilon n_3}{5} - \frac{n_0}{10} + \frac{n_2}{5} + \frac{y_2 y_3}{2} - \frac{9 \ln y_1}{5} \right) + \left(-\frac{\epsilon n_3}{5} + \frac{n_2}{10} + \frac{3y_4 y_5}{10} + \frac{-\frac{n_0}{10} - \frac{n_1}{5} + \frac{n_2}{10}}{5y_9} + \frac{y_6 y_7}{5} \right) \\ & \left(-\frac{\epsilon n_3}{5} + \frac{n_2}{10} + \frac{2y_4 y_5}{5} + \frac{-\frac{n_0}{10} - \frac{n_1}{5} + \frac{n_2}{10}}{5y_9} + \frac{y_6 y_7}{5} + \frac{e^{y_8}}{10} - \frac{1}{10} \right) \\ & + e^{\frac{y_2 y_3}{5} - \frac{3y_6 y_7}{10}} + \ln \left(\frac{y_2 y_3}{10} + 1 \right) - 1 \end{aligned} \quad (6)$$

with

$$\begin{aligned} y_0 &= -\frac{\epsilon n_3}{5} + \frac{n_2}{10}, \quad y_1 = -\frac{7n_1}{10} - \frac{7n_2}{10} + 1, \quad y_2 = \frac{3\epsilon n_5}{10} - \frac{2n_0}{5} + \frac{n_2}{10}, \quad y_3 = \frac{2\epsilon n_4}{5} - \frac{2\epsilon n_5}{5} - \frac{n_1}{10} - \frac{n_2}{10}, \\ y_4 &= -\frac{3n_0}{10} - \frac{n_1}{2} + \frac{3n_2}{10}, \quad y_5 = \frac{2n_0}{5} + \frac{2n_1}{5} - \frac{3n_2}{10}, \quad y_6 = -\frac{\epsilon n_5}{5} - \frac{3n_0}{10} - \frac{2n_1}{5} + \frac{3n_2}{10}, \\ y_7 &= \frac{\epsilon n_5}{2} + \frac{n_0}{10} + \frac{2n_1}{5} - \frac{n_2}{5}, \quad y_8 = \frac{n_0}{10} - \frac{3n_1}{10} - \frac{3n_2}{5}, \quad y_9 = -\frac{3n_0}{10} - \frac{n_1}{2} + \frac{n_2}{10} + 1 \end{aligned}$$

and convolution kernels ω_i shown in Fig.4c

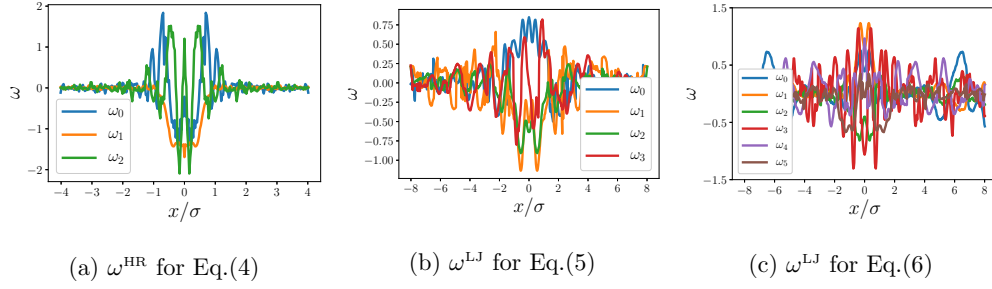


FIG. 4: ω for all cases. (a)HR. (b)LJ, splitting. (c)LJ, no splitting. The maximum allowed range for the kernels is $[-4\sigma, 4\sigma]$ in the HR case and $[-8\sigma, 8\sigma]$ in the LJ case.

IV. FEQL BUILDING AND PHYSICAL CONSTRAINTS

To build FEQL, we first use *SymPy*⁵ to determine \mathcal{F}^{ML} and $\frac{\partial \mathcal{F}^{\text{ML}}}{\partial n_i}$ with a given number of weighted densities n_w , levels and nodes. Second, we feed the $\frac{\partial \mathcal{F}^{\text{ML}}}{\partial n_i}$ and trainable parameters into *Tensorflow*⁶; then add other layers to fit the DFT structure (convolutions and Eq.(4) in the main paper). Finally, the network is trained by *Keras*⁷ with *Tensorflow* backend.

Since \mathcal{F}^{ML} approximates \mathcal{F}^{ex} , we must consider two physical constraints: (i) $\mathcal{F}^{\text{ML}}(\rho = 0) = 0$ and (ii) $\left. \frac{\delta \mathcal{F}^{\text{ML}}}{\delta \rho} \right|_{\rho=0} = 0$. To enforce (i), we choose the linear mapping without bias and $f(0) = g(0, z) = 0$ in the non-linear mapping. Condition (ii) can be enforced by setting appropriate parameters from the matrix $W^{(l)}$ of the final level to zero. This requires to determine the analytic form of $\left. \frac{\partial \mathcal{F}^{\text{ML}}}{\partial n_i} \right|_{\rho=0}$ to identify those parameters. For example, for a FEQL with $n_w = 2$, 2 levels and (1,1,1,1,1) nodes nodes for (identity, exponential, logarithm,

multiplication and division),

$$\begin{aligned}
f^{\text{ML}} = & a_2 L_0 (a_1 L_0 n_0 + a_1 L_1 n_1) + a_2 L_1 \left(e^{a_1 L_2 n_0 + a_1 L_3 n_1} - 1 \right) + a_2 L_2 \ln (a_1 L_4 n_0 + a_1 L_5 n_1 + 1) + a_2 L_3 (a_1 L_6 n_0 + a_1 L_7 n_1) (a_1 L_8 n_0 + a_1 L_9 n_1) \\
& + \frac{a_2 L_4 (a_1 L_{10} n_0 + a_1 L_{11} n_1)}{a_1 L_{12} n_0 + a_1 L_{13} n_1 + 1} + \left(a_2 L_{15} (a_1 L_0 n_0 + a_1 L_1 n_1) + a_2 L_{16} \left(e^{a_1 L_2 n_0 + a_1 L_3 n_1} - 1 \right) + a_2 L_{17} \ln (a_1 L_4 n_0 + a_1 L_5 n_1 + 1) \right) + \\
& a_2 L_{18} (a_1 L_6 n_0 + a_1 L_7 n_1) (a_1 L_8 n_0 + a_1 L_9 n_1) + \frac{a_2 L_{19} (a_1 L_{10} n_0 + a_1 L_{11} n_1)}{a_1 L_{12} n_0 + a_1 L_{13} n_1 + 1} \left(a_2 L_{20} (a_1 L_0 n_0 + a_1 L_1 n_1) + a_2 L_{21} \left(e^{a_1 L_2 n_0 + a_1 L_3 n_1} - 1 \right) \right) \\
& + a_2 L_{22} \ln (a_1 L_4 n_0 + a_1 L_5 n_1 + 1) + a_2 L_{23} (a_1 L_6 n_0 + a_1 L_7 n_1) (a_1 L_8 n_0 + a_1 L_9 n_1) + \frac{a_2 L_{24} (a_1 L_{10} n_0 + a_1 L_{11} n_1)}{a_1 L_{12} n_0 + a_1 L_{13} n_1 + 1} \left. \right) + \\
& \left(a_2 L_{25} (a_1 L_0 n_0 + a_1 L_1 n_1) + a_2 L_{26} \left(e^{a_1 L_2 n_0 + a_1 L_3 n_1} - 1 \right) + a_2 L_{27} \ln (a_1 L_4 n_0 + a_1 L_5 n_1 + 1) + a_2 L_{28} (a_1 L_6 n_0 + a_1 L_7 n_1) \right. \\
& \left. (a_1 L_8 n_0 + a_1 L_9 n_1) + \frac{a_2 L_{29} (a_1 L_{10} n_0 + a_1 L_{11} n_1)}{a_1 L_{12} n_0 + a_1 L_{13} n_1 + 1} \right) / \left(a_2 L_{30} (a_1 L_0 n_0 + a_1 L_1 n_1) + a_2 L_{31} \left(e^{a_1 L_2 n_0 + a_1 L_3 n_1} - 1 \right) + \right. \\
& \left. a_2 L_{32} \ln (a_1 L_4 n_0 + a_1 L_5 n_1 + 1) + a_2 L_{33} (a_1 L_6 n_0 + a_1 L_7 n_1) (a_1 L_8 n_0 + a_1 L_9 n_1) + \frac{a_2 L_{34} (a_1 L_{10} n_0 + a_1 L_{11} n_1)}{a_1 L_{12} n_0 + a_1 L_{13} n_1 + 1} + 1 \right) + \\
& e^{a_2 L_5 (a_1 L_0 n_0 + a_1 L_1 n_1) + a_2 L_6 (e^{a_1 L_2 n_0 + a_1 L_3 n_1} - 1) + a_2 L_7 \ln (a_1 L_4 n_0 + a_1 L_5 n_1 + 1) + a_2 L_8 (a_1 L_6 n_0 + a_1 L_7 n_1) (a_1 L_8 n_0 + a_1 L_9 n_1) + \frac{a_2 L_9 (a_1 L_{10} n_0 + a_1 L_{11} n_1)}{a_1 L_{12} n_0 + a_1 L_{13} n_1 + 1}} \\
& + \ln \left(a_2 L_{10} (a_1 L_0 n_0 + a_1 L_1 n_1) + a_2 L_{11} \left(e^{a_1 L_2 n_0 + a_1 L_3 n_1} - 1 \right) + a_2 L_{12} \ln (a_1 L_4 n_0 + a_1 L_5 n_1 + 1) + \right. \\
& \left. a_2 L_{13} (a_1 L_6 n_0 + a_1 L_7 n_1) (a_1 L_8 n_0 + a_1 L_9 n_1) + \frac{a_2 L_{14} (a_1 L_{10} n_0 + a_1 L_{11} n_1)}{a_1 L_{12} n_0 + a_1 L_{13} n_1 + 1} + 1 \right) - 1
\end{aligned}$$

with $a_x L_y$ the y -th parameter in $W^{(x)}$. Then we calculate $\left. \frac{\partial f^{\text{ML}}}{\partial n_i} \right|_{\rho=0}$, such as

$$\begin{aligned}
\left. \frac{\partial f^{\text{ML}}}{\partial n_0} \right|_{\rho=0} = & a_1 L_0 a_2 L_0 + a_1 L_0 a_2 L_{10} + a_1 L_0 a_2 L_{25} + a_1 L_0 a_2 L_5 + a_1 L_{10} a_2 L_{14} + a_1 L_{10} a_2 L_{29} + a_1 L_{10} a_2 L_4 + a_1 L_{10} a_2 L_9 \\
& + a_1 L_2 a_2 L_1 + a_1 L_2 a_2 L_{11} + a_1 L_2 a_2 L_{26} + a_1 L_2 a_2 L_6 + a_1 L_4 a_2 L_{12} + a_1 L_4 a_2 L_2 + a_1 L_4 a_2 L_{27} + a_1 L_4 a_2 L_7
\end{aligned}$$

and

$$\begin{aligned}
\left. \frac{\partial f^{\text{ML}}}{\partial n_1} \right|_{\rho=0} = & a_1 L_1 a_2 L_0 + a_1 L_1 a_2 L_{10} + a_1 L_1 a_2 L_{25} + a_1 L_1 a_2 L_5 + a_1 L_{11} a_2 L_{14} + a_1 L_{11} a_2 L_{29} + a_1 L_{11} a_2 L_4 + a_1 L_{11} a_2 L_9 \\
& + a_1 L_3 a_2 L_1 + a_1 L_3 a_2 L_{11} + a_1 L_3 a_2 L_{26} + a_1 L_3 a_2 L_6 + a_1 L_5 a_2 L_{12} + a_1 L_5 a_2 L_2 + a_1 L_5 a_2 L_{27} + a_1 L_5 a_2 L_7
\end{aligned}$$

Thus we set $a_2 L_{11}$, $a_2 L_{29}$, $a_2 L_2$, $a_2 L_{26}$, $a_2 L_{25}$, $a_2 L_9$, $a_2 L_{12}$, $a_2 L_7$, $a_2 L_{27}$, $a_2 L_5$, $a_2 L_4$, $a_2 L_{10}$, $a_2 L_{14}$, $a_2 L_1$, $a_2 L_6$ and $a_2 L_0$ to zero in order to keep $\left. \frac{\delta \mathcal{F}^{\text{ML}}}{\delta \rho} \right|_{\rho=0} = 0$.

REFERENCES

- ¹J. K. Percus, J. Stat. Phys. **15**, 505 (1976).
- ²R. Roth, J. Phys. Condens. Matter **22**, 063102 (2010).
- ³R. Tibshirani, J. R. Stat. Soc. Series B Stat. Methodol. , 267 (1996).
- ⁴P. Mehta, M. Bukov, C.-H. Wang, A. G. Day, C. Richardson, C. K. Fisher, and D. J. Schwab, Phys. Rep. (2019).

⁵Meurer *et al.*, PeerJ Comput. Sci. **3**, e103 (2017).

⁶M. Abadi *et al.*, “TensorFlow: Large-scale machine learning on heterogeneous systems,” (2015), software available from tensorflow.org.

⁷F. Chollet *et al.*, “Keras,” <https://keras.io> (2015).